JOINT EUROPEAN TORUS

JET-P(89)56

J.P. Christiansen and J.G. Cordey

The Role of Current Profile Broadening in L and H-Mode Plasmas

"This document is intended for publication in the open literature. It is made available on the understanding that it may not be further circulated and extracts or references may not be published prior to publication of the original when applicable, or without the consent of the Publications Officer, EFDA, Culham Science Centre, Abingdon, Oxon, OX14 3DB, UK."

"Enquiries about Copyright and reproduction should be addressed to the Publications Officer, EFDA, Culham Science Centre, Abingdon, Oxon, OX14 3DB, UK."

The contents of this preprint and all other JET EFDA Preprints and Conference Papers are available to view online free at www.iop.org/Jet. This site has full search facilities and e-mail alert options. The diagrams contained within the PDFs on this site are hyperlinked from the year 1996 onwards.

The Role of Current Profile Broadening in L and H-Mode Plasmas

J.P. Christiansen and J.G. Cordey

JET Joint Undertaking, Culham Science Centre, OX14 3DB, Abingdon, UK

Preprint of a paper to be submitted for publication in
Nuclear Fusion

JET-P(89)56

THE ROLE OF CURRENT PROFILE BROADENING IN L AND H-MODE PLASMAS

by

J.P. Christiansen and J.G. Cordey

JET Joint Undertaking, Abingdon, Oxon, OX14 3EA, U.K.

Preprint of a paper to be submitted for publication in Nuclear Fusion

August 1989

The Role of Current Profile Broadening in L and H-mode Plasmas

J P Christiansen and J G Cordey
JET Joint Undertaking, Abingdon, Oxon, OX14 3EA

ABSTRACT

Auxiliary heating by neutral beams (NBI) or ion cyclotron resonance heating (ICRH) can broaden or peak the plasma current density profile. A measure of changes to the current density profile J_ϕ is established by a combination of current moments which yields a profile broadening parameter ζ. JET experiments are demonstrated to increase ζ (broaden J_ϕ) when NBI is applied to discharges which exhibit either L or H mode confinement; pellet injection and ICRH are demonstrated to decrease ζ (peak J_ϕ). The time evolution of the parameter ζ is shown to correlate with the changes to the D_α emission seen in H-mode discharges with and without ELMs. The broadening of J_ϕ by NBI, especially for H-mode pulses, starts in the edge region. It is caused by the non-inductive bootstrap current component as a consequence of steep density profiles. The ohmic current component undergoes only a nominal change. Associated with current profile broadening is an increase in edge pressure and total stored plasma energy W. An analysis of global confinement (variations of W with power P) is made by splitting W into three parts: W_f, the fast ion energy; W_1, the edge energy which is empirically shown to be proportional to the current profile broadening parameter ζ; W_p, the bulk plasma thermal energy. It is shown that the scaling for W_p in the L and H-mode confinement regimes is similar.

1. INTRODUCTION

Experiments on JET with fixed plasma geometry and with fixed values of toroidal current I_ϕ and field B_ϕ show considerable variations in confinement properties: at a fixed level of input power P the total stored plasma energy W can be as much as 2.5 times the smallest value found at that power level. The input power includes ohmic heating, neutral beam injection (NBI) heating and ion cyclotron resonance frequency (ICRF) heating while the stored plasma energy includes thermal energy and energy of fast ions produced by NBI and/or ICRH. Figure 1 shows data on W and P from a series of JET pulses with I_ϕ = 3MA, B_ϕ = 3T; the plasma configurations in these pulses have a separatrix inside the JET vessel and are referred to as double null (DN) or

single null (SN) plasmas. The plasmas have either NBI or ICRF heating or both applied and the data values are measured at the time t_{max}, when the peak value W_{max} is obtained during a pulse. At $t = t_{max}$, dW/dt approaches zero such that the values W_{max} and P approximate steady state data; each JET pulse is thus represented by only one data point. It is clear from the scatter of the data in Fig. 1 that it becomes difficult to establish a scaling law for the energy W or for the global confinement time $\tau_E = W/(P-dW/dt)$. This is especially true since the only parameter which is varied in the data shown in Fig. 1 is the average density $\langle n \rangle$ of the target plasma to which varying amounts of P(NBI) or P(ICRH) have been applied. The spread of data values arises from: i) sawteeth effects, ii) variations in power deposition profiles and fast ion energy content, iii) edge plasma physics and iv) the varying conditions of the JET plasma vessel. Such effects do not depend on plasma parameters in any simple way which would permit deduced scaling laws $W = W(P,\langle n \rangle)$ or $\tau_E = \tau_E(P,\langle n \rangle)$, to be identified with one or more plasma physics loss mechanisms.

If data from pulses with different values of current I_ϕ or field B_ϕ is included then the effects from sawteeth will tend to conceal the dependence of W upon I_ϕ and P since both the sawtooth inversion radius and the period τ_s will vary. This makes it difficult to unravel intrinsic confinement properties such as local or average ion-electron thermal diffusivities χ_e, χ_i from global data. Figure 1 does indeed emphasise this difficulty.

A detailed examination of the data in Fig. 1 reveals that it is possible to divide the plasma pulses into three groups. The first group exhibits uninterupted H-mode confinement for periods longer than a confinement time and the data presented from the group is marked by a full circle in the figures of this paper. H-mode confinement was first established on the ASDEX experiment [1] and later found on the Doublet III [2], PDX [3], JET [4], JFT-2M and DIII-D experiments. The H-mode confinement regime is characterised by a spontaneous reduction of D_α (or H_α) emission from the plasma edge region. Sometimes this reduction is interrupted by intermittent bursts of D_α emission caused by ELMs [6]. The ELMs last only a fraction of the global confinement time τ_E suggesting that the intermittent changes from L-mode to H-mode confinement occur only in the edge region while the bulk plasma region remains unaffected. JET pulses exhibiting ELMs form the second group of pulses and their data is marked by open circles in the figures of this paper. The third group of pulses marked by crosses have L-mode confinement whose scaling has been the subject of many studies, e.g. [5].

The solid line in Fig. 1 has been calculated from the scaling law given in [5] and is only shown for guidance. The three groups of data points in Fig. 1 emphasize the considerable variation in total stored plasma energy W that can be achieved at a given power level.

The difference in W between H and L-mode plasmas has been ascribed to an edge or pedestal energy in refs. [8]. By separating the edge energy from the total energy for JET H-mode plasmas it has been found that the difference representing the bulk plasma energy shows a scaling with power which is similar to L-modes [8]. The work presented in this paper is an extension of [8], but with a different approach to determine the edge energy. Section 6 explains how the total energy W for JET L and H modes (i.e. the data of Fig. 1) can be split into three parts: W_f, the fast ion energy produced by ICRH or NBI; W_p, the bulk plasma thermal energy; W_l, the edge energy proportional to a parameter ζ. This parameter characterizes the broadening of the current profile due to auxiliary heating and the first part of the paper (sections 2 to 5) describes this in detail. The last part of the paper deals with the impact on global confinement of current profile changes.

Changes to the plasma current profile are by definition associated with changes to the internal inductance ℓ_i. Determination of ℓ_i from magnetic measurements requires a model for the current distribution. Experience from applying 2 different models to JET data shows that presently the accuracy (or confidence level) of ℓ_i in the range $0.9 < \ell_i < 1.5$ is of order 0.05 to 0.1. The changes $\Delta \ell_i$ due to auxiliary heating observed from these two models range from -0.15 to 0.15, i.e. of order of the accuracy. Thus changes in ℓ_i cannot in the work presented reliably be used to measure current profile broadening.

We have chosen to measure the broadening (or peaking) of the plasma current profile $\langle J_\phi(x) \rangle$ via a parameter ζ which represents a combination of changes to current moments Y_m that are model-independent and have an accuracy level of order 5%. The brackets $\langle\ \rangle$ refer to an average at a plasma surface x, where x is a non-dimensional flux surface label, $0 \le x \le 1$, used throughout this paper. The next section explains the use of current moments.

Section 3 describes data from JET experiments in which the auxiliary heating is demonstrated to either broaden J_ϕ ($\zeta>0$) or contract or peak J_ϕ ($\zeta<0$). Changes to the moments Y_m are most pronounced during the L to H-mode transition as shown in Section 4; this is due to the strong weighting towards the edge of the moments Y_m. The changes to Y_m and hence J_ϕ are identified with the bootstrap current [7] in Section 5; the ohmic part of J_ϕ undergoes only a minor change.

Section 6 shows how the increment ΔW due to auxiliary heating can be identified with increments to the three parts of W mentioned above. For plasmas with L-mode confinement the broadening parameter ζ is small (or negative) and the energy increment ΔW comes mainly from increments to the thermal energy W_p and fast ion energy W_f. For plasmas with H-mode comfinement ζ is large and ΔW arises mainly from the edge energy W_1. The latter is found to correlate with the parameter ζ. This correlation enables us to combine L-mode and H-mode scaling : section 6 extends the analysis of [8] by showing that the bulk thermal energy W_p has approximately the same scaling in L and H-mode plasmas. The intrinsic local confinement properties, i.e. the diffusivity χ, should therefore be similar in L and H-mode plasmas over the bulk of the plasma. The bulk in this context refers to $0 < x < x_B$, where x_B will vary from plasma pulse to plasma pulse. Although x_B remains undetermined it is expected to lie in the range $0.8 < x_B < 1$.

The characterization of confinement presented in this paper is based on un-ambiguous measures of moments of the plasma current distribution. It allows us to assess the current profile broadening in L and H-mode confinement. It does not, however, identify the cause of the L to H-mode transition during which τ_E is observed to increase. The improved confinement in the H-mode can be caused by a variety of plasma effects as described in [1-4], [6] and [8]; section 6 includes a short discussion.

2. CURRENT MOMENTS

The current moments most often used to characterise a current distribution are those defined by Zakharov and Shafranov [9]. These moments are defined as

$$Y_m = \frac{1}{\mu_o I_\phi} \int F_m \, B_p \, dl = \frac{1}{I_\phi} \int F_m \, J_\phi \, da \, , \qquad (1)$$

where the contour integral is evaluated along a flux surface; B_p is the poloidal field and J_ϕ is the plasma current density. The weighting functions satisfy

$$\nabla \times \nabla \times F_m \hat{e}_\phi = 0 \ , \tag{2}$$

$\hat{e}_\phi$ being a unit vector in the ϕ direction of a (R,ϕ,Z) co-ordinate system. The choice of solutions to (2) made in reference [9] is based on making two moments Y_1 and Y_{1_Z} vanish

$$Y_1 = \frac{1}{\mu_0 I_\phi} \int F_1 \, B_p dl \equiv 0, \; Y_{1_Z} = \frac{1}{\mu_0 I_\phi} \int F_{1_Z} \, B_p dl \equiv 0 \ . \tag{3}$$

The functions entering (3) are (R_0 is, eg, torus centre)

$$F_1^0 = (R-R_0)(1 + \frac{R-R_0}{2R_0}) \ , \quad F_{1_Z}^0 = Z$$

and Eq(3) defines the coordinates (R_J, Z_J) of the current channel centre

$$R_J = (2Y_1 \, R_0 + R_0^2)^{1/2}, \qquad Z_J = Y_{1_Z} \ .$$

The weighting functions F_m, which are solutions to Eq.(2) in toroidal geometry, can be expressed in terms of the following two functions containing the parameter R_J

$$F_1 = (R-R_J) \ (1+ \frac{R-R_J}{2R_J}), \quad F_{1_Z} = Z \ (1+ \frac{R-R_J}{R_J}).$$

For m = 2, 3, 4 we have

$$\begin{aligned} F_2 &= F_1^2 - F_{1_Z}^2 \ , \quad F_3 = F_1^3 - 3F_1 F_{1_Z}^2 + \frac{Z^2}{R_J} F_{1_Z}^2 \ , \\ F_4 &= F_1^4 - 6 \, F_1^2 \, F_{1_Z}^2 + F_1^2 (3F_1^2 - 2Z^2) - \frac{4}{5} \frac{Z^4}{R_J^2} F_1^2 \ . \end{aligned} \tag{4}$$

The moments Y_m for m=0 to 4 have routinely been evaluated from Eq.(1) for all JET plasma pulses since the start of operation. These moments describe mainly the current distribution in the outermost part of the plasma, since the functions (4) vary approximately as $x^m \cos m\theta$; x denotes, as mentioned earlier, a normalised flux surface label and θ is a poloidal angle. A moment Y_m by itself does not describe the spatial profile shape $\langle J_\phi(x) \rangle$ of an equilibrium current distribution

$$\langle J_\phi \rangle = \langle R \frac{dp}{d\psi} + \frac{1}{\mu_0 R} f \frac{df}{d\psi} \rangle \qquad (5)$$

in which p is total pressure, $f = RB_\phi$ and ψ poloidal flux. To see this we can evaluate e.g. Y_2 for plasma equilibria whose flux surface geometry is described by shifted ellipses, i.e. by two functions S(x) and E(x) respectively. The expression for J_ϕ or B_p derived in ref. [10] together with Eq.(4) gives

$$Y_2 = - a^2 \left(\frac{E_1^2-1}{4E_1^2} - \lambda_1 \frac{E_1^4+3E_1^2-2}{4E_1^2}\right) + O(\epsilon,S). \qquad (6)$$

Eq.(6) a is minor radius, $\epsilon = a/R$, $E_1 = E(x=1)$ and $\lambda_1 = \lambda(x=1)$, where $\lambda = x \frac{1}{E} \frac{dE}{dX}$. Eq.(6) shows us that Y_2 and similarly Y_3, Y_4..., can each be varied independently by appropriate changes to the external magnetic field (plasma cross section shaping). When the spatial profile shape $\langle J_\phi(x) \rangle$ changes <u>all</u> moments must change.

We can consider a perturbation δJ_ϕ (Eq. 5) varying as $\frac{\partial}{\partial x} \delta(x-x_B)$, where δ denotes the delta function. The resulting changes to the current moments will then vary as $\Delta Y_m \sim (m+1)\, x_B^m$. An appropriate measure of current profile broadening would then be

$$\zeta = \sum_{m=2}^{M} d_m \frac{\Delta Y_m}{a^m} \gamma_m, \qquad d_m = m+1, \qquad (7)$$

where γ_m represents a phase factor from integration in the poloidal direction. In practice the changes $\delta J_\phi(x)$ have finite spatial extent such that the coefficients d_m in (7) would not be equal to m+1. The choice (7) adopted in this paper with $d_2 = -3$, $d_3 = 4$, is by no means unique; the key point is the combination of changes to the moments. These changes are calculated as

$$\Delta Y_m = Y_m\,(t) - Y_m\,(\text{ohmic}) \qquad (8)$$

in which ohmic refers to a value before the start of additional heating. The significance of the choice (7) can be seen in the JET data described in the next section. To illustrate how changes to the current profile can be measured we show in Figure 2 the time variation ζ (t) for three different JET pulse scenarios. The first pulse (#17380) with ζ increasing (broadening of $\langle J_\phi(x) \rangle$) exhibits H-mode confinement during NBI heating. The second pulse

(#16209) has pellet injection some 0.1 sec. prior to NBI and ICRF heating during the current rise phase. In this phase the moments Y_m undergo substantial changes as the current profile itself peaks by resistive diffusion towards a steady state profile. The marginal peaking of J_ϕ for this pulse is therefore represented as the difference in $\zeta(t)$ between pulse 16209 and a previous pulse 16201 with no pellet, NBI and ICRH. Peaking of J_ϕ is pronounced during the current decay phase as illustrated for pulse 15954 in Figure 2. The functions (4) weight J_ϕ by x^{m+1}. If a pellet penetrates close to the axis and changes J_ϕ at say $x = \frac{1}{4}$, then the resulting change to Y_2 is only $^1/_{64}$ of that due to broadening of J_ϕ by NBI at $x = 1$. Figure 2 emphasizes such a difference.

3. CURRENT PROFILE CHANGES IN JET EXPERIMENTS

We have analysed data from 500 JET pulses with plasma current and field of 3MA and 3T respectively. Various plasma configurations have been used in these JET pulses: for plasmas attached to the inner wall or the upper-lower belt limiters minor radius and ellipticity have been varied; plasma shapes whose boundary form an internal separatrix can be made up-down symmetric (double-null) or asymmetric (single null). The auxiliary heating power has been varied with combinations of NBI (21MW maximum) and ICRH (15MW maximum). The changes to the J_ϕ profile caused by auxiliary heating can be clearly demonstrated in plots of ΔY_3 vs ΔY_2 such as those shown in Figures 3a and b. ΔY is calculated from Eq.(8) for each JET pulse at a time when $W = W_{max}$, i.e. the same time t_{max} used for the W vs P data in Fig. 1. Fig. 3a shows for a series of ICRF heated plasmas that the central power deposition produces negligible changes ΔY_m; in these deuterium plasmas the He^3 minority ions transfer energy mainly to the electrons. Fig. 3a also includes data selected from ICRH and NBI heated limiter plasmas with single or multiple pellet injection during the current rise phase [11]. In such experiments the current profile is being peaked or broadened by the combination of pellets and NBI-ICRH. The scatter of the data arises from a range of different scenarios adopted in these experiments: i) the time of pellet injection is varied from the current rise phase to the current flat top period, ii) the ratio of ICRH to NBI power is varied and iii) the penetration of the pellet varies, i.e. the value of x_B at which the density profile steepens, varies. For the pellet pulses ΔY_m represent the change due to pellets, NBI, ICRH since the change caused by resistive diffusion during the current rise has been subtracted as explained in the previous section.

Fig. 3b show on the other hand quite clearly how ΔY_m undergo significant changes as a result of NBI heating. The data in Fig. 3b originates from DN and SN plasma configurations with up to 21MW of NBI. Pulses exhibiting H-mode confinement, H-mode confinement with ELMs and L-mode confinement are marked as in Fig. 1. The current profile broadening (changes to ΔY_2 and ΔY_3) is most pronounced for pulses with H-mode and H-mode + ELMs. The data on ΔY_2 and ΔY_3 show how these have been varied gradually in the JET experiments. It is from plots like Fig. 3b and from linear regression analyses of the data on ΔY_m that a combination of moments such as that of Eq.(7) has emerged as a useful and simple representation of current profile broadening.

4. THE TRANSITION FROM L TO H-MODE CONFINEMENT

The transition from L to H-mode confinement [12] and similarly the reverse transition (H to L) is characterised by rapid changes over a period of 10^{-3} to 10^{-2} secs. in the D_α emission. Such rapid changes can occur intermittently and they are accompanied by changes to the current profile. In Figure 4 we show the time variations $D_\alpha(t)$ and ζ (t) for JET pulse 15954 which exhibits H-mode confinement with ELMS. The current profile broadens continuously until the occurrence of the first ELM at 55.3 secs. While the bursts of D_α are correlated with rapid changes to the broadening parameter ζ, there is no clear indicator (e.g. threshold value) in ζ (t) which indicates the onset of H-mode confinement. The lack of distinction is illustrated in Figure 5 by plots of ζ (t) for 7 successive JET pulses with H-mode confinement and for one pulse with L-mode confinement. The onset of the H-mode for these particular pulses occurs in the time interval 0.2 - 0.4 sec after application of NBI. At the L to H-mode transition there is a change in the slope $d\zeta/dt$; this can be seen in Fig. 5 and more clearly in Fig. 4. Similarly at the H to L-mode transition (marked by a rapid increase in D_α emission) the slope $d\zeta/dt$ changes abruptly and ζ then gradually decreases over a period of up to 2 secs. The termination of the H-mode (as derived from D_α) is rapid and it can occur at various values of ζ, one of which is marked by an arrow in Figure 5.

The time evolution of ζ is governed by resistive diffusion. The approximate width Δ over which the resistive diffusion changes J_ϕ is

$$\Delta = (\eta/\mu_0\ (t-t_{NB}))^{\frac{1}{2}} \approx 0.22\ g^{\frac{1}{2}}\ T_e^{-\frac{3}{4}}\ (t-t_{NB})^{\frac{1}{2}}, \qquad (9)$$

in which T_e is in units keV, g is the neoclassical correction to η caused by trapped electrons and $Z_{eff} = 3$, $\ln \Lambda = 15$. The time variation of ζ will depend on the details of the equilibrium profiles $\frac{dp}{d\psi}$ and $\frac{df}{d\psi}$ of Eq.(5). For small perturbations to J_ϕ ζ will vary like

$$\zeta \sim c_1\ x_B^2 \Delta + c_2\ x_B\ \Delta^2 + c_3\ \Delta^3 \qquad (10)$$

in which c_1 to c_3 are same constants and x_B the flux surface at which broadening takes place. Eqs.(9-10) mimic the time variation of ζ seen in Fig. 5.

Rapid changes to ζ such as those of Fig. 4 will according to Eq.(9) involve changes over a narrow width of order 0.02 - 0.05m if $T_e \approx$ 1keV. The results in Figs. 4 and 5 suggest that the L to H and H to L-mode transitions are marked by rapid changes to J_ϕ within a narrow boundary layer i.e. at x_B close to 1. After the L to H transition the remaining part of the current profile continues to broaden and after the H to L transition J_ϕ relaxes towards its L-mode shape, both these processes occurring on a longer timescale.

5. PROFILE CHANGES

The changes to profiles of density, temperature, current density and pressure caused by neutral beam heating have been studied for a set of double null plasma configurations; the set of pulses concerned include 43 pulses with L-mode and 34 pulses with H-mode confinement. For this set, which is a subset of the pulses whose data is shown in Figs. 1 and 3, density and temperature profiles by the JET LIDAR diagnostic have been measured close to the time t_{max} when $W=W_{max}$. Fig 6 shows the density and temperature profiles normalised to the axial values and averaged over the L and H-mode set of pulses. While the electron temperature T_e is only marginally broader for H than for L-modes there is pronounced difference between the corresponding density profiles. The difference suggests that the change to J_ϕ as seen in the curves for ζ (t) is associated with density or density gradients rather than temperature or temperature gradients.

The relationship between temperature and current density is given by ohms law

$$\frac{1}{\eta} E_\phi = J_\phi - J_\phi^{NI} \tag{11}$$

J_ϕ is the total current density used to define Y_m and ζ. J_ϕ^{NI} refers to the non-inductive part which includes bootstrap and beam driven currents [13]. The analysis of identifying the measured values of ΔY_2, ΔY_3 etc with either J_ϕ^{NI} or changes to $\frac{1}{\eta} E_\phi$ proceeds as follows. We estimate the changes to the ohmic current density and to the bootstrap current density from

$$\delta Y_2^{OH} = \frac{1}{I_\phi} \Delta \left(\int_0^1 \frac{1}{\eta} E_\phi F_2 \, x dx\right), \tag{12a}$$

$$\delta Y_2^{NI} = \frac{1}{I_\phi} \Delta \left(\int_0^1 J_\phi^{NI} F_2 \, x dx\right). \tag{12b}$$

The bootstrap current density is given by a surface average parallel to the field [7,13,14]

$$\left\langle \frac{1}{R} J_\phi^{NI} \right\rangle + \frac{1}{f} \langle \underline{J}_p^{NI} . \underline{B}_p \rangle = - \frac{(\epsilon x)^{1/2}}{\psi'} \left(\alpha_1 T_e \frac{dn_e}{dx} + \alpha_2 n_e \frac{dT_e}{dx} + \alpha_3 n_e \frac{dT_i}{dx}\right) \tag{13}$$

The dimensionless coefficients α_1-α_3 depend on the atomic $\langle Z \rangle$, on the plasma surface geometry and on the degree of collisionality and $\psi' = \frac{d\psi}{dx}$ is proportional to B_p. The dominant contribution in (13) comes from the α_1 term.

Figures 7a and 7b show respectively the calculated values of δY_2^{OH} and δY_2^{NI} versus the measured values of ΔY_2. Each point represents the value in one of the 43 L and 34 H mode pulses at a time t(LIDAR) chosen as close as possible to t_{max}. Since the difference between t_{max} and t(LIDAR) can be up to 1 sec the values of ΔY_2 used for the comparison with δY_2^{OH} and δY_2^{NI} are calculated at t = t(LIDAR). This means that the values of ΔY_2 in Figs. 7a and 7b are not the same values as those of Fig. 3b. Fig. 7a shows no correlation between δY_2^{OH} and ΔY_2; this can be expected qualitatively since the T_e profiles for L and H-modes of Figure 6 do not differ greatly. Fig. 7b shows on the other hand a measure of agreement between δY_2^{NI} and the measurement ΔY_2. A similar agreement is formed between δY_3^{NI} and δY_3 although in both cases it would appear that the theoretical value of α_1 is $\sim$50% too large.

6. ENERGY INCREMENTS FROM CURRENT PROFILE BROADENING

The broadening of the current profile $\langle J_\phi(x)\rangle$ has been demonstrated in many JET experiments; it can be achieved at constant total current by a current control feedback system. The non-inductive component, i.e. the bootstrap current, causes in feedback mode a reduction of the voltage at the plasma edge. This is described in more detail in reference [13].

On JET the NBI geometry is such that the pressure of the 80keV fast ions (D) remains almost isotropic [13]. The energy of the minority ions to which the ICRH is coupled is on the other hand perpendicular energy which can be in excess of 1 MeV per minority ion (H or He^3). These fast ions slow down and transfer energy to both the plasma electrons and ions; expressions for the characteristic slowing down times can be found in ref. [15]. The increment ΔW to the total stored plasma energy resulting from NBI and or ICRH can therefore be written as the sum

$$\Delta W = W_{NBI} + W_{RF} + W_{thermal} \tag{14}$$

In equation (14) the first term represents the energy of the fast ion population due to NBI

$$W_{NBI} = \left(A^e_{NBI} \frac{T_{eo}}{\langle n_e\rangle}^{3/2} + A^i_{NBI} \frac{1}{\langle n_e\rangle}\right) P_{NBI} \tag{15}$$

The coefficients A^e_{NBI} and A^i_{NBI} depend on the ratio E_b/eT_e where E_b is the beam energy. For JET E_b = 80keV. The second term in Eq. (14) represents the energy of fast ions due to ICRH

$$W_{RF} = A_{RF} \frac{T_{eo}}{n_{eo}}^{3/2} P_{RF}, \tag{16}$$

The expressions (15-16) are approximate since the NBI and ICRH deposition profiles need to be determined. The use of the average density $\langle n_e\rangle$ in (15) and the axial density n_{eo} in (16) reflects that NBI deposition profiles are broader than the ICRH profiles. Eqs. (15-16) show that the fast ion energy content $W_f = W_{NBI} + W_{RF}$ is significant only for large values of $T_e^{3/2}/n_e$ (L-mode) plasmas). W_{RF} can in JET exceed 2MJ while W_{NBI} can be of order 0.1 - 0.3 MJ. In (15-16) T_{eo} is in units keV and n_e in units 10^{19} m^{-3}.

The third term in Eq. (14) represents the increase in thermal plasma energy due to auxiliary heating. This increase caused by the slowing down of fast ions depend on both the power deposition profiles and the plasma loss processes [16]. We characterize it by two parts

$$W_{thermal} = W_p + W_1 \tag{17}$$

the first being the increase out to some plasma surface x_B, the second representing the increase from x_B to the plasma edge. For L-mode plasmas only Wp is significant while in H-mode confinement regimes W_1 is the dominant part of ΔW. The extent of the region $x_B \leq x \leq 1$ in which the improved confinement is present during the H-mode will vary from pulse to pulse, just as the degree of current profile broadening varies, i.e. the parameter ζ. In this region the change to the thermal energy for $n_e = n_i = n$, $T_e = T_i = T$ is approximately

$$W_1 \approx \int_{x_B}^{1} \Delta\ (3enT)\ R\tau dx \tag{18a}$$

while the parameter ζ due to the bootstrap current becomes

$$\zeta \approx \int_{x_B}^{1} \alpha_1\ T\ \frac{dn}{dx}\ (\sum_m F_m)\ \tau dx \tag{18b}$$

In Eqs. (18) τdx is the area element between x and x + dx. Partial integration of (18b) shows us that the parameter ζ is a weighted measure of the energy increment, i.e. for x_B close to 1 the approximate relation can be derived

$$W_1 \approx C_1\ \zeta + C_2 \approx \Sigma D_m\ \Delta Y_m \tag{18c}$$

in which C_1, C_2 and D_m are some constants.

Such a proportionality is demonstrated empirically in the JET data by the correlation between the time evolution of ΔW and ζ. Figure 8 shows the correlation for the sequence of 7 H-mode pulses used also in Fig.4. Figure 8 demonstrates that the energy increment ΔW obtained in H-mode pulses is proportional to the current profile broadening parameter. The curves in Figure 8 track ΔW and ζ from the time $t=t_{NBI}$ (start of NBI) to t_{max} when $W=W_{max}$.

Having established the proportionality between ζ and ΔW we can now characterize the global confinement for the 190 L-mode pulses and 124 H-mode pulses, whose data is shown in Fig. 1, by

$$W = W_{OH} + W_{NBI} + W_{RF} + W_p + W_1 \qquad (19)$$

W_{OH} refers to the value in the ohmic heating phase prior to auxiliary heating and W_{NBI} and W_{RF} are given by Eqs. (15-16). The bulk plasma thermal energy increase is

$$W_p = \tau_{inc} \left(P - \frac{dW}{dt}\right) \qquad (20)$$

in which the incremental confinement time t_{inc} is related to an effective diffusivity χ and heating efficiency as described in reference [16]. The edge energy increase we express in view of (18c) by

$$W_1 = \sum_{m=z}^{4} A_m \Delta Y_m \qquad (21)$$

rather than by $A\zeta$. As mentioned in section 2 the choice made in this paper of the coefficients d_m in the definition (Eq. 7) of ζ is not unique; Eq. (21) offers a better description of the JET data than $W_1 = A\zeta$ does.

Regression analyses have been carried out by fitting the JET data on W to the expression (19). In these regression analysis calculations we allow the parameters A_2, A_3, A_4, τ_{inc}, A^e_{NBI}, A^i_{NBI} and A_{RF} to be varied. A variety of calculations are performed, eg, $A_3 = 0$, $A_3 = A_4 = 0$, etc. The best fit is obtained by setting $A^e_{NBI} = A^i_{NBI} = A_{NBI}$ and allowing A_2, A_3, A_4 to be determined separately. The result is

$$A_{NBI} = (3.5 \pm 1)10^{-3},\ A_{RF} = (1.3 \pm 0.1)10^{-2},\ \tau_{inc} = 0.17 \pm 0.01\ (s)$$

$$A_2 = 110 \pm 6\ ,\quad A_3 = -29 \pm 5\ ,\quad A_4 = 27 \pm 3.$$

The scatter in the fit of W_T to the data W defined as the r.m.s. of the relative error is only 11%. The result is illustrated by a plot similar to Figure 1 of the bulk thermal energy W_p versus $P - \frac{dW}{dt}$. Such a plot is shown in Fig. 9 for the L and H-mode data of Fig. 1. The solid line represents

the L-mode scaling [5] and it is again only included for guidance; a linear offset scaling can equally well represent the data of Fig. 9. Fig. 9 clearly demonstrates that the large departures from the scaling seen in Fig. 1 can be identified with the expressions (14-21). The variation of W_p with $P - \frac{dW}{dt}$ suggests that all pulses (L and H-modes) exhibit the same confinement (τ_{inc}) in the bulk of the plasma, $0 \leq x \geq x_B \approx 0.8 - 1$. Fig. 10 shows the fast ion energy content W_f plotted against $T_e^{3/2}/n_{eo}$ rather than against input power. Only L-mode plasmas have significant fast ion energy. The edge energy W_1 calculated from Eq.(21) is shown in Fig. 11 plotted against the profile parameter ζ given by Eq.(7). Even though the coefficients A_m are not related like the coefficients d_m of Eq.(7) the correlation between W_1 and ζ is good. This correlation corresponds to the proportionality between ΔY_2 and ΔY_3 (Fig. 3b) and similarly between ΔY_2 and ΔY_4 (not shown in this paper). The edge energy W_1 is not proportional to the total input power (and neither is ζ), but rather to the power deposition profile which will vary from pulse to pulse. The characterisation of W_1 by Eqs.(18) and (21) through weighted integrals shows that the improved confinement in the H-mode regime takes place in the outer region as suggested in [8]. Presently the extent of this region, ie, $x_B < x < 1$, cannot be determined directly but only via moments of J_ϕ. The large variations of W at fixed P as seen in Fig. 1 are therefore identified for L-mode plasmas mainly with W_f and for H-mode plasmas with W_1. It is also emphasized that we cannot distinguish between cause and effect as regards the L to H mode confinement transition itself.

The analysis [16] uses the following expression for the total heat flux q

$$q = -en\,\chi\,\langle\nabla T\rangle + q_{pinch}$$

The heat pinch term satisfies the Onsager symmetry principle relating heat fluxes, particle fluxes and current density. If the latter is modified by a bootstrap current proportional to $T\,\langle\nabla n\rangle$ so too should the heat and particle fluxes be modified. Whether the confinement in the H-mode is improved by the heat pinch itself, by χ being a function of $T\,\nabla n$ or by the current profile broadening, cannot yet be clearly demonstrated. In the case of JET a high spatial resolution of n and T measurements in the edge region is required to experimentally establish the parametric dependencies of the heat pinch over a wide range of plasma conditions and if so, which functional form of χ represents both L and H-mode confinement.

Global confinement analysis has previously (e.g. [5]) established a dependence of the confinement time (or its incremental value) upon the total plasma current. The present work suggests that the plasma current profile shape is also important.

CONCLUSION

In this paper we have proposed a method for examining the changes to the plasma current density profile caused by auxillary heating. This method is based on un-ambiguous current moments and should prove useful to assess the role of lower-hybrid current drive. We have identified the broadening of the current density profile, especially for H-mode plasmas, with the presence of a bootstrap current in the edge region. By splitting the total stored energy into three parts, the fast ion energy, the edge energy proportional to the current profile broadening parameter and the bulk thermal plasma energy W_p, we have shown that the confinement properties (W_p vs P) in the bulk of the plasma are similar for a large number of JET L and H-mode plasmas; the improved H-mode confinement takes place in the outer region of the plasma. This characterization of confinement data does however not distinguish between cause and effect as regards the L to H-mode transition.

ACKNOWLEDGEMENTS

The authors wish to thank the JET team for making the data available for analysis. The work by K Thomsen on the JET transport database is gratefully acknowledged. The calculations of the moments due to the bootstrap current have been carried out by D O'Brien and G Corrigan. The authors wish to thank Dr. M. Keilhacker for the effort spent on improvements to this paper.

REFERENCES

[1] WAGNER, F., BECKER, K., BEHRINGER, K., CAMPBELL, D. et al.

Proc. 9th IAEA conf. on Plasma Physics and Contr. Nucl. Fusion Research, Baltimore 1982, Vol.I, IAEA, Vienna (1982) 43.

[2] BURRELL, K.,

Proc. 11th European Conf. on Controlled Fusion and Plasma Physics, Aachen 1983, Vol 1, (1983) 11.

[3] KAYE, S.M., BELL, M., BOL, K., BOYD, D., et al. ibid Vol 1(1983)19.

[4] TANGA, A., BARTLETT, D., BEHRINGER, K., BICKERTON, R.J., et al.

Proc. 11th IAEA Conf. on Plasma Physics and Contr. Nucl. Fusion Research, Kyoto 1986, Vol. IAEA Vienna (1986).

[5] GOLDSTON, R.J., Plasma Physics and Controlled Fusion, 26(1984)87.

[6] KEILHACKER, M., BECKER, G., BERNHARDE, K., EBERHAGEN, A., et al., Plasma Physics and Controlled Fusion, 26(1984)49.

[7] BICKERTON, R.J., CONNOR, J.W., TAYLOR, J.B., Nature Phys. Sci. 229(1971)110.

[8] KEILHACKER, M., and the JET team, The JET H-mode at high current and power levels, 12th IAEA Conf. on Plasma Physics and Contr. Nucl. Fusion Research, Nice 1988, IAEA-CN-50/A-III-2.

THOMSEN, K., CALLEN, J.D., CHRISTIANSEN, J.P., CORDEY, J.G., et al. Offset-linear description of H-mode confinement, 16th Europ. Conf. on Controlled Fusion and Plasma Physics (Venice, Italy) (1989), Europhysics Conference Abstracts, Vol.13b, Part III p.223.

[9] ZAKHAROV, L.E., SHAFRANOV, V.E., Sov. Tech. Phys. 18(1973)151.

[10] CHRISTIANSEN, J.P., CALLEN, J.D., ELLIS, J.J., GRANETZ, R., Nucl. Fusion 29(1989)703.

REFERENCES cont.

[11] SCHMIDT, G.L. and the JET Team, Heating of peaked density profiles produced by pellet injection in JET, 12th IAEA Conf. on Plasma Physics and Contr. Nucl. Fusion Research, Nice 1988, IAEA-CN-50/A-IV-1.

[12] CARLSTROM, T.N., SHIMADA, M., BURRELL, K.H., DeBoo, J., et al. H-mode transition studies in DIII-D, 16th Europ. Conf. on Controlled Fusion and Plasma Physics (Venice, Italy) (1989), Europhysics Conference Abstracts, Vol. 133, Part I, p.241.

[13] CHALLIS, C.D., CORDEY, J.G., HAMNÉN, H., STUBBERFIELD, P.M., et al. Nucl. Fusion 29(1989)563.

[14] HIRSHMAN, S.P., SIGMAR, J., Nucl. Fusion 21(1981) 1079.
KIM, Y.B., CALLEN, J.D., HAMNÉN, H., (1988) JET Report R(88)02.

[15] WESSON, J.A., Tokamaks, Oxford Science Publications, Clarendon Press, Oxford (1987).

[16] CALLEN, J.D., CHRISTIANSEN, J.P., CORDEY, J.G., THOMAS, P.R., THOMSEN, K., Nucl. Fusion 27(1987)1857.

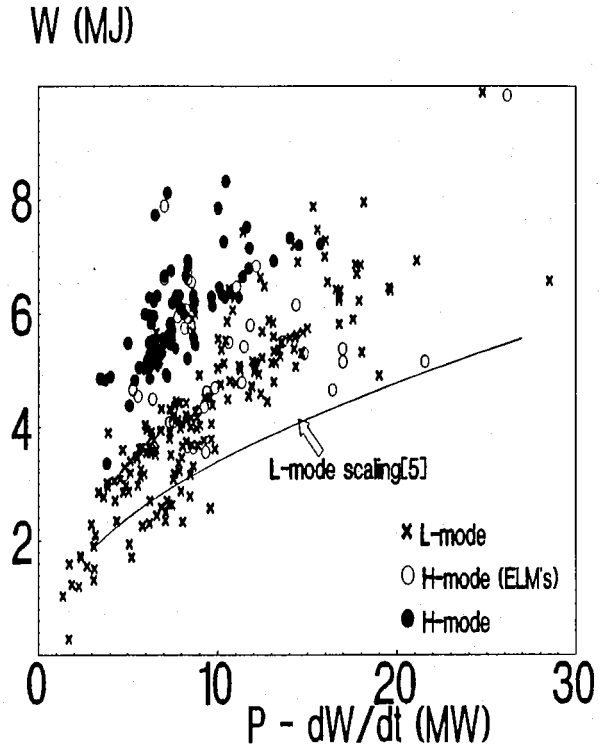

FIG. 1. The total stored plasma energy W determined from diamagnetic loop measurements vs input power-dW/dt. Data values are for 3MA, 3T DN and SN plasmas. 190 pulses have L-mode, 124 have H-mode confinement (39 with ELM's).

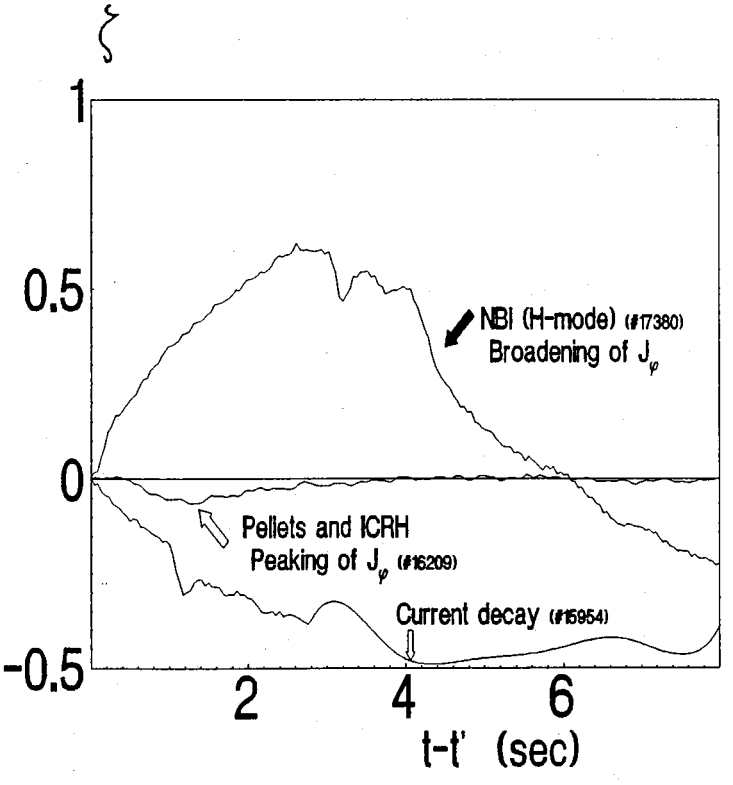

FIG. 2. Time evolution of the profile broadening parameter parameter ζ (Eq.7) for three representative JET pulses. t' is the time with NBI start (#17380), pellet (#16209) and start of current decay (#15954).

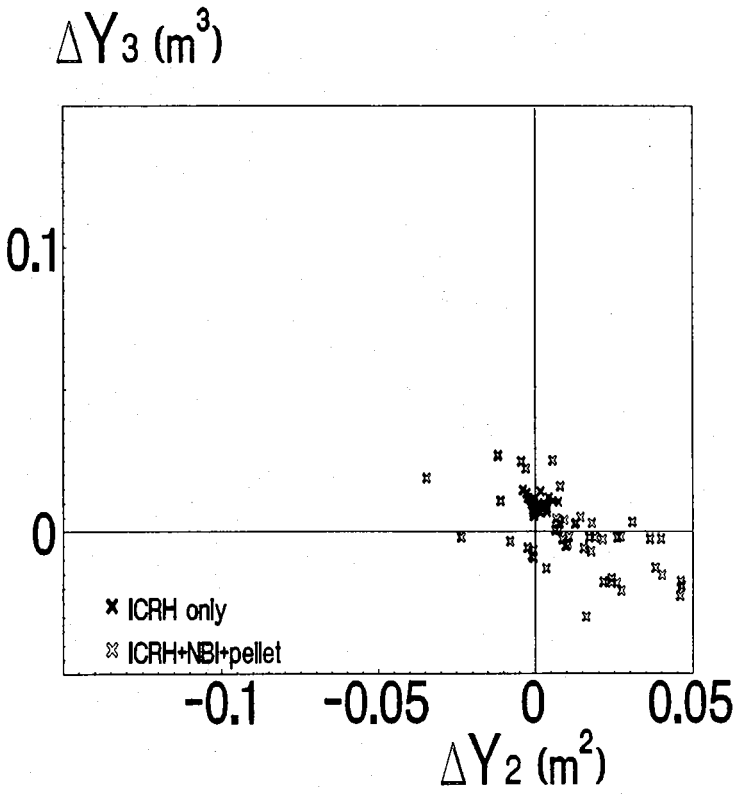

FIG. 3a. Changes to the 3rd vs changes to the 2nd current moments (Eq.8). Pulses with ICRH only show no detectable changes to the current profile. With ICRH+NBI+pellets the current profile can be either peaked or broadened.

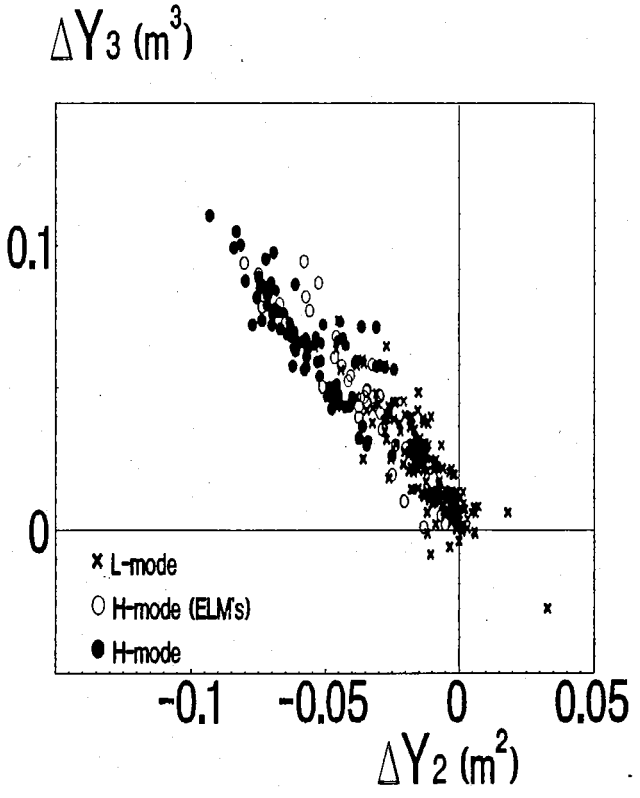

FIG. 3b. Changes to the 3rd vs changes to the 2nd current moments (Eq.8) for the JET pulses used in figure 1. Most H-mode and some L-mode plasmas exhibit significant current profile broadening.

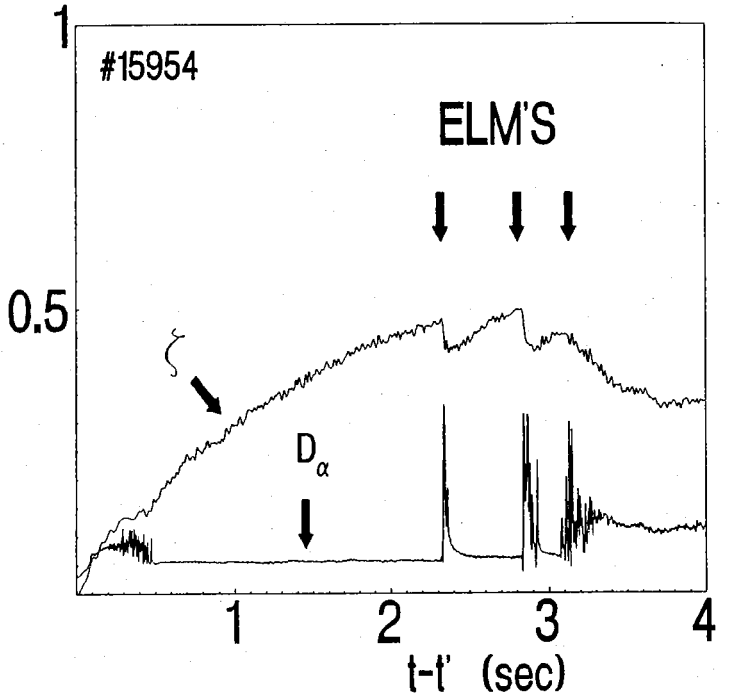

FIG. 4. Increases and decreases to the profile broadening parameter ζ and to the D_α emission caused by ELMs during a period with H-mode confinement. t' is start of NBI.

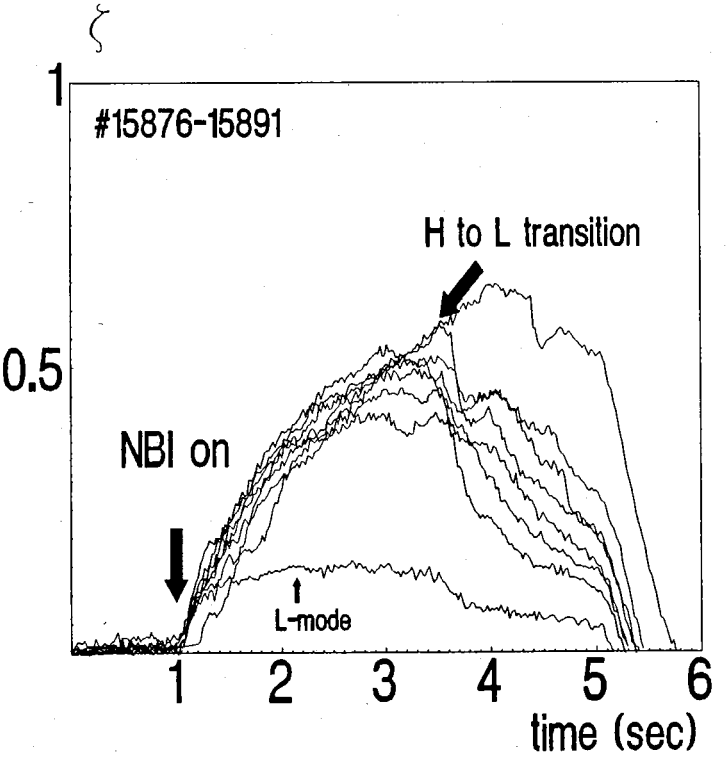

FIG. 5. Time evolution of the profile broadening parameter ζ for a sequence of one L-mode and 7 H-mode pulses. The H to L transition for one pulse is arrowed.

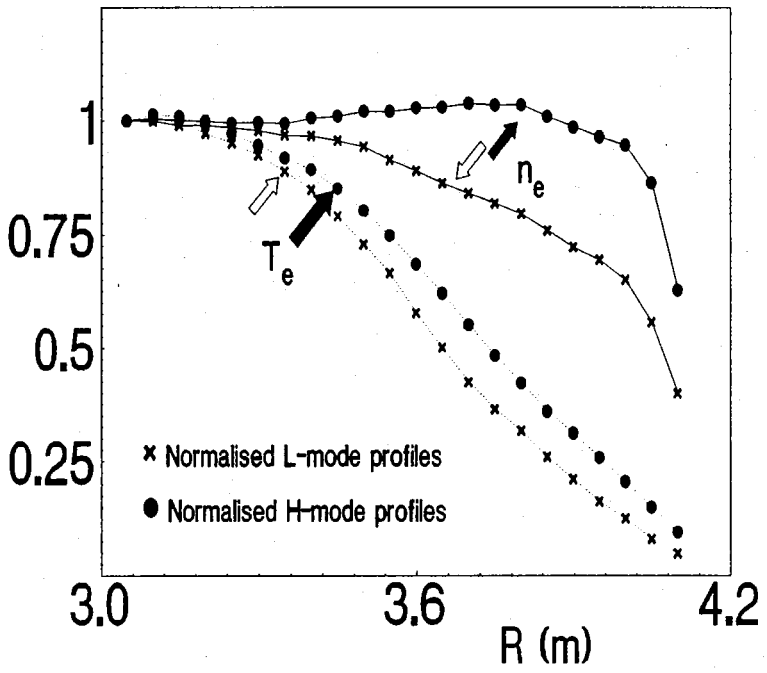

FIG. 6. Average of normalised electron density and temperature profiles measured by LIDAR. The average is made of 43 L-mode and 34 H-mode pulses.

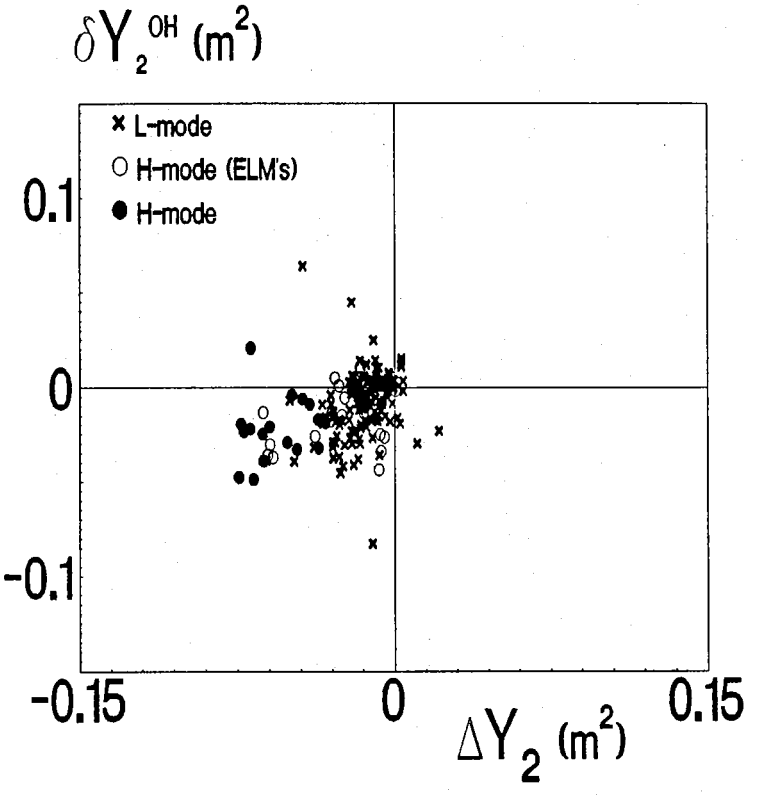

FIG. 7a. The estimated change to Y_2 due to the ohmic current does not correlate with the measured change.

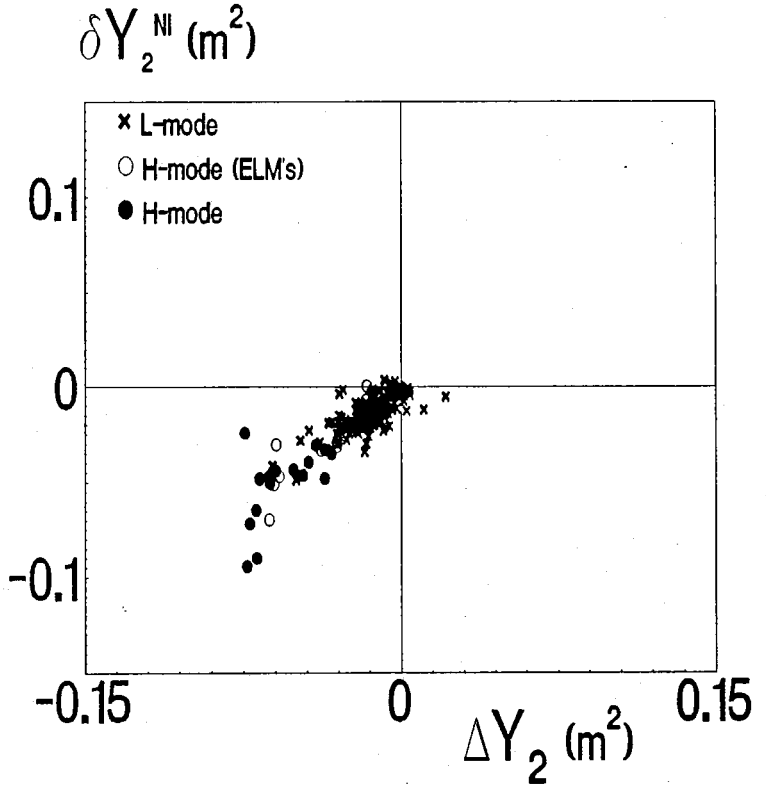

FIG. 7b. The estimated change to Y_2 due to the bootstrap current is correlated with the measured change.

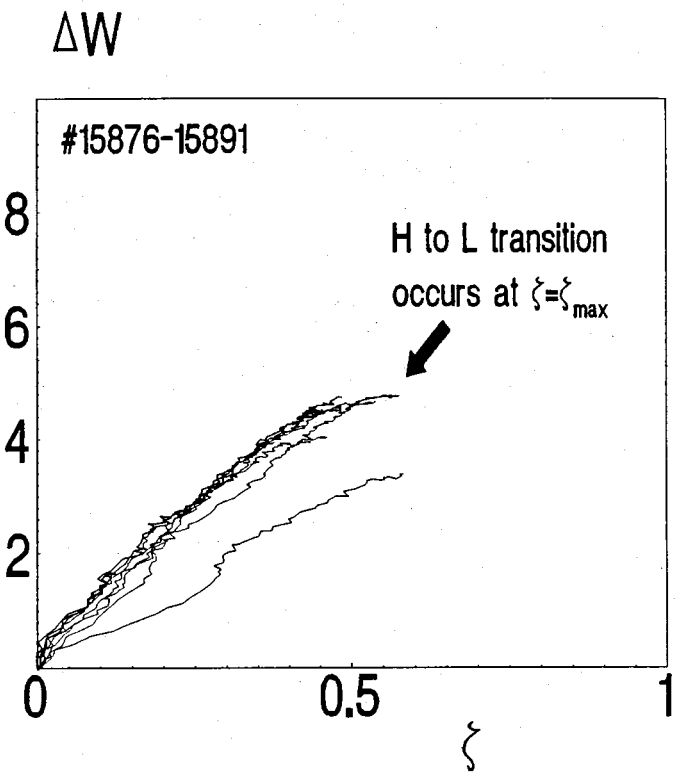

FIG. 8. The increase in total stored energy is seen to be proportional to the current profile broadening parameter ζ for 7 pulses exhibiting H–mode confinement.

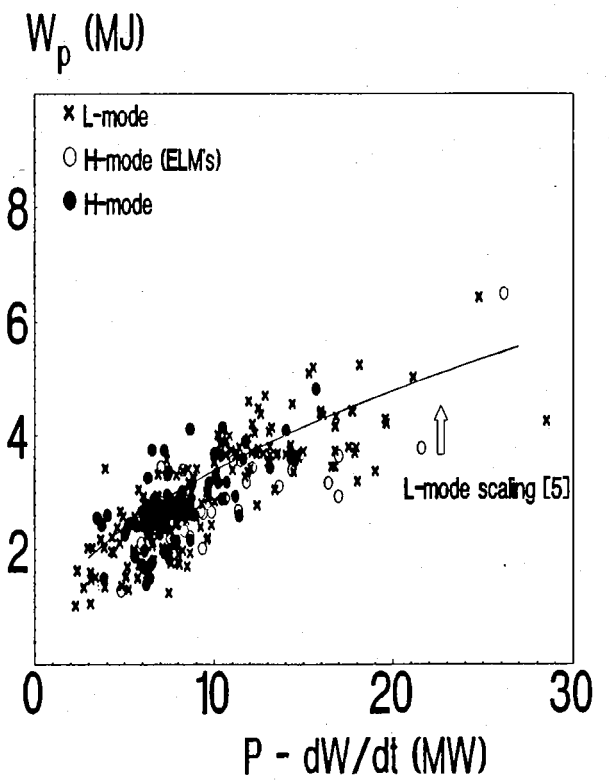

FIG. 9. The thermal energy of the bulk plasma derived from regression analysis shows a power dependence which is similar in L and H–mode confinement regimes.

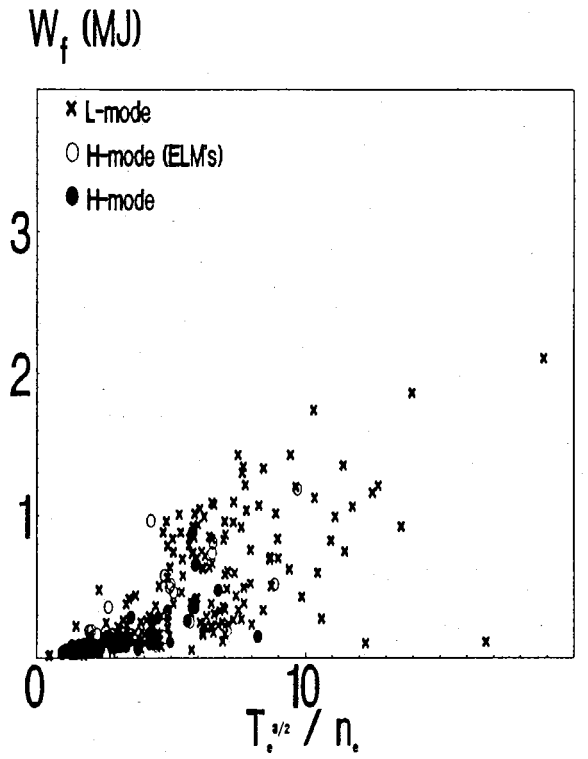

FIG. 10. The fast ion energy derived from regression analysis does not scale with power input. It is therefore shown versus $T_e^{3/2} / n_e$

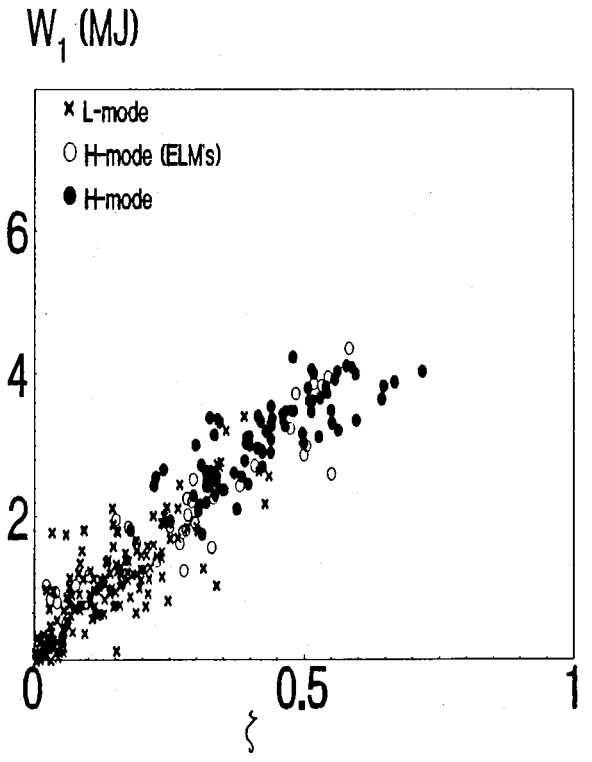

FIG. 11. The edge energy derived from regression analysis is proportional to the current profile broadening parameter ζ *defined by Eq.(7)*